Microsyst Technol (2012) 18:849–856
DOI 10.1007/s00542-011-1387-7

TECHNICAL PAPER

Thermopile-based THz antenna

Béla Szentpáli · Gábor Matyi · Péter Fürjes · Endre László · Gábor Battistig · István Bársony · Gergely Károlyi · Tibor Berceli

Received: 29 July 2011 / Accepted: 23 November 2011 / Published online: 3 December 2011

Abstract This work is intended to describe the design aspects and to characterize the functionality of a novel thermopile structure applicable for detecting millimetre range and THz radiation. The proposed thermopile consists of a series of micromachined poly-crystalline silicon thermocouple strips arranged linearly. This device can act as a series of antennas; its antenna-like operation was demonstrated clearly by the strong polarization dependence when detecting microwave radiation. The sensing principle is similar to the basic operation of bolometers in that the absorbed radiation heats up the semiconductor strips, but the temperature increment is detected by the Seebeck effect instead of the resistance change. Therefore there is no read-out current and the voltage output starts from zero. In the present work we are going to show the simulation of the current distribution. The fabrication of the device will also be outlined, as well as the results of measurements performed at 13, 100 GHz, and both in broad-band THz and in infrared radiation.

B. Szentpáli (✉) · P. Fürjes · E. László · G. Battistig · I. Bársony
Research Institute for Technical Physics and Materials Science of the Hungarian Academy of Sciences, P.O. Box 49, Budapest 1525, Hungary
e-mail: szentpali@mfa.kfki.hu

G. Matyi
EnerSys Advanced Systems, Gyár u. 2, Budaörs 2040, Hungary

G. Károlyi · T. Berceli
Department of Broadband Infocommunications and Electromagnetic Theory, Budapest University of Technology and Economics, Goldmann György tér 3, Budapest 1111, Hungary

1 Introduction

The thermoelectric effect which is also referred to as Seebeck effect after the discoverer, is extensively utilized for temperature measurement by wire thermocouples. Thermopiles multiply the output signal by connecting many thermocouples in series. Due to the dynamic development of the micromachining technologies these devices are manufactured using these techniques since the early 90's years. The sketch of a MEMS thermopile is shown in Fig. 1a. The thermocouples lie on a thin dielectric membrane grown on Si substrate, which is etched out from the middle region. Primarily it is used for sensing infrared radiation (Graf et al. 2007). Due to the excellent thermal isolation of the membrane the absorbed power heats up the inner ends of the thermocouple loops, while the outer ends are thermalized by the substrate to the ambient temperature. This great asymmetry of the heat conduction is the key point of the device. The device can be equipped with an electric heater strip at the centre of the membrane, enabling it to measure the gas flow-rate, through the convective cooling of the heater (Dijkstra et al. 2008); in addition to this construction is an electronic device realizing Quadratic Transfer Characteristics (Szabó and Székely 2009). Regarding THz and mid-infrared radiation, the thermopiles were used only for the read-out the temperature increment caused by absorption of radiation in the feed-point resistance of the metallic antenna (Chong and Ahmed 1997), or in the thin-film absorber (Kasalynas et al. 2007).

Another construction for sensing mm waves and THz radiation was suggested by the authors (Szentpáli et al. 2010). In this case the thermocouples are arranged linearly instead of loops, as it is sketched in Fig. 1b. Here the thermocouple strips act as short circuited dipole antennas.

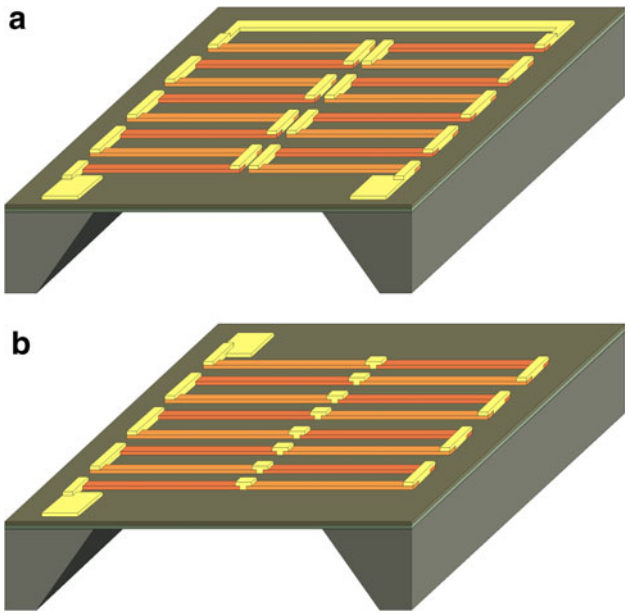

Fig. 1 **a** The outline of the MEMS thermopile. In some constructions there is a heater on the membrane between the two group of loops. **b** The linear arrangement of the thermopairs

The high-frequency electric field parallel to them induces currents and Joule heating in them. The current distribution has a maximum value at the centre and zero at the ends of the strips. Therefore the heat formation peaks around the middle of the lines, exactly where it generates the highest thermoelectric effect.

In the present work the fabrication of the device is briefly outlined and then functionality is examined by electromagnetic modelling. These results are compared to the available measurements. The variations in the results of the measurements are (partially) the result of certain aspects of the encapsulation.

2 Fabrication

In order to achieve a reliable fabrication process, the conventional poly-silicon thermopile technology was combined and improved by double side bulk silicon micromachining (Graf et al. 2007; Seidel et al. 1990; Vázsonyi et al. 2003). For enhanced mechanical stability the residual stress in the suspended membrane was reduced by applying a stacked layer structure containing a double layer of non-stochiometric silicon–nitride (SiN_x) and silicon-oxide (SiO_2) with the appropriate thickness ratio (Resnik et al. 2004). The main steps of the process are shown in Fig. 2. A low stress SiN_x layer was deposited on the silicon substrate using low pressure chemical vapour deposition (LPCVD) at 830°C temperature and by applying a SiH_2Cl_2:NH_3 = 4:1 gas mixture within this process. To reduce the stress in the 700 nm thick silicon–nitride membrane, a 200 nm thick SiO_2 layer was deposited on top of it using an atmospheric CVD process with a SiH_4 precursor at the temperature of 450°C. A 400 nm thick functional poly-silicon layer was deposited using a LPCVD process at 630°C with SiH_4 as the precursor and subsequently etched for the given geometry (10 μm wide poly-silicon strips) defined by the lithography. Ion implantation of boron and phosphorus ions at 40 keV was used for setting the p and n doping of the poly-silicon stripes. It was followed by the double step annealing process (600 and 1,050°C) which resulted in 23.7 and 37 Ω/□ sheet resistance for n and p type poly-silicon, respectively. The contact pads and the wiring was structured from evaporated Al. KOH backside anisotropic alkaline etching at 78°C temperature was used to remove the substrate underneath the membrane. Finally the wafers were diced and the chips were mounted on the prototype panels. The photos of two chips fabricated on the same wafer are shown in Fig. 3a and b. The thermopile in Fig. 3a consists of

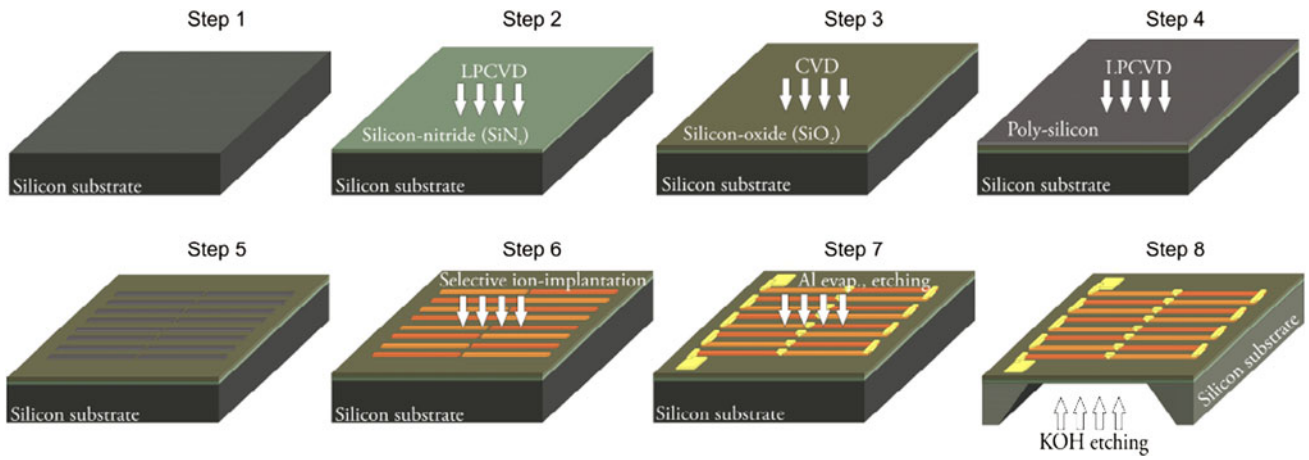

Fig. 2 The principal process flow of the fabrication of the device

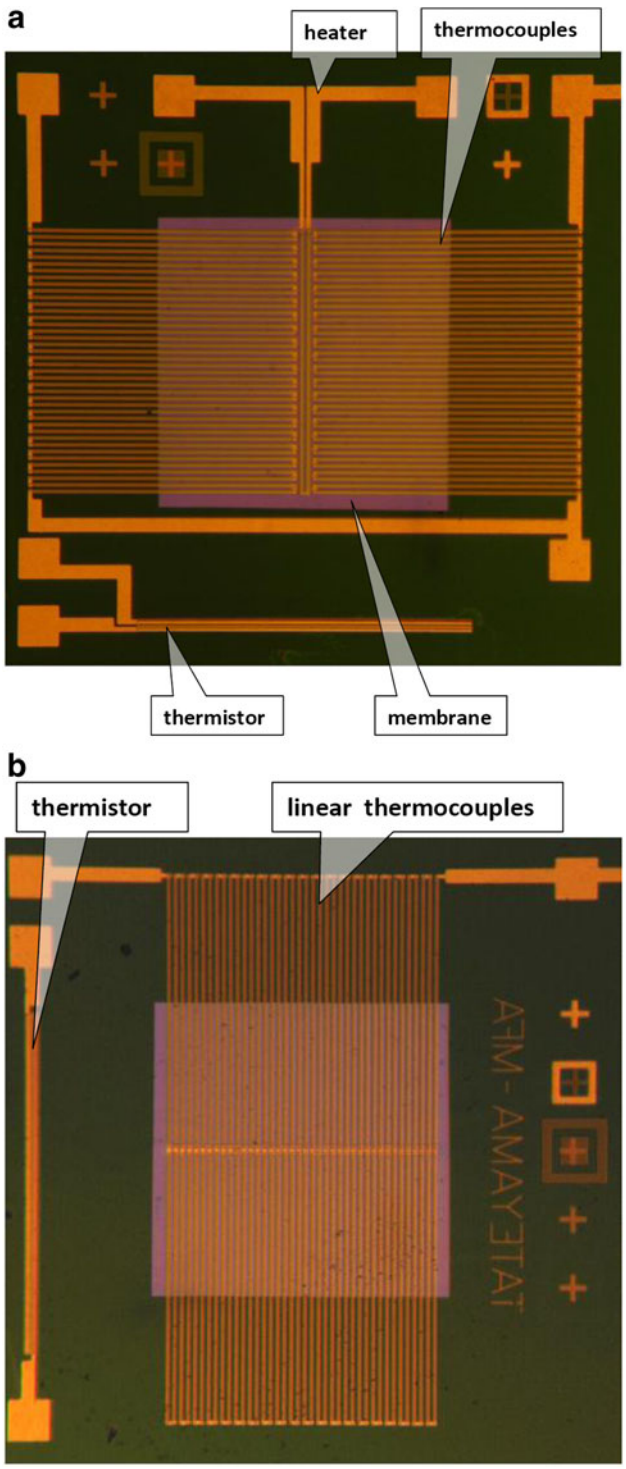

Fig. 3 **a** The photo of the thermopile with loops and heater. **b** The photo of the linear thermopile. The chip size in both cases is 2×2 mm^2

thermocouple loops and a poly-silicon heater between the loops. The thermopile in Fig. 3 b is made up of linearly arranged p and n type poly-silicon strips.

3 Full wave electromagnetic model

The sensing mechanism was characterized by full wave electromagnetic simulation. To reduce the calculation time the simulated model was simplified to a certain extent, the cross-section with the dimensions are shown in Fig. 4. This simplification does not affect the principle of the operation. The CST Microwave Office^{TM}. code was employed for the simulations. The THz electric field was always parallel to the thermocouple lines and the value of the induced current in the mid-point (in the Al contact) was calculated as the function of the frequency in case of different geometries. The value of the contact resistance was 1 Ω, roughly equal to the DC contact resistance. The simulation results were practically the same when this value was varied between 0.5 and 3 Ω. At first a single thermopile strip was analyzed as a resonant dipole antenna surrounded only by vacuum, the result is shown as spectrum "a" in Fig. 5. The simulation results in only one resonance peak, close to 200 GHz, which is somewhat lower than the frequency of the free space radiation having a half wavelength equal to the antenna length. This shift can be attributed to the resonance loss, which can explain the relatively small and very broad peak too. The second and third order harmonics completely disappeared. As this thermopile strip was placed onto the top of the supporting membrane structure at the centre of the air filled cavity, the first order resonance shifted strongly downwards to ~90 GHz, and it became narrower, and its amplitude increased. Higher order peaks appeared too, as the spectrum "b" presents in Fig. 5. The shift of the peak can be explained by the enhancement of the electric length of the antenna due to the high dielectric constant of the substrate. As a rule of thumb the effective ε of the surrounding medium of the antenna can be estimated trough the relative volume ratio of the air and the silicon. In this way the value of 5.59 can be derived, which results in 84.7 GHz instead of 200 due to the wavelength shortening. This effect is the cause of the enhancement of the equivalent area of the antenna, for which the peak is higher by as much as the relative increase of the wavelength. The radiation induces resonant modes in the cavity system through the enclosing apertures as well. The peaks at higher frequencies are probably due to these cavity resonances.

The complete structure was also simulated, where 48 parallel thermocouple strips almost completely cover the slot in the substrate. The results are shown in Fig. 6. Each strip line has its own individual current spectrum. The amplitude and the bandwidth of the first order resonance peak are higher at the sides than in the centre. In the centre part, the first order resonance peak is still the greatest but not dominant compared to the further resonant peaks at higher frequencies. It seems that the central dipoles receive

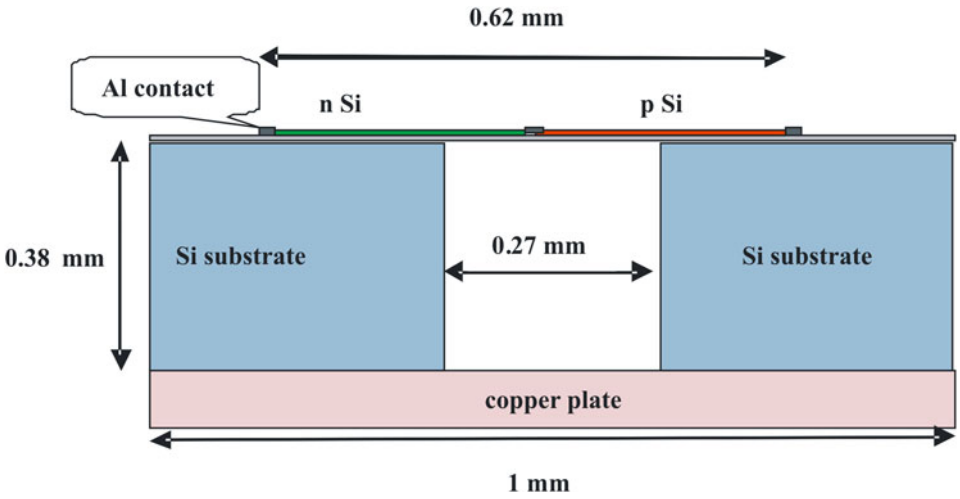

Fig. 4 The dimensions of the simulated structure. The chip is 1×1 mm^2, the inner hole is 0.27 mm wide and 0.83 mm long, the thickness of the dielectric membrane is 0.9 μm. The poly Si strips are 10 μm wide and 0.4 μm thick, the specific conductivity is 5×10^4 S/m for both type. The spacing between them is 5 μm. The Al contacts are 10 μm wide. In the course of some simulations the cooper plate was substituted by a dielectric printed circuit board

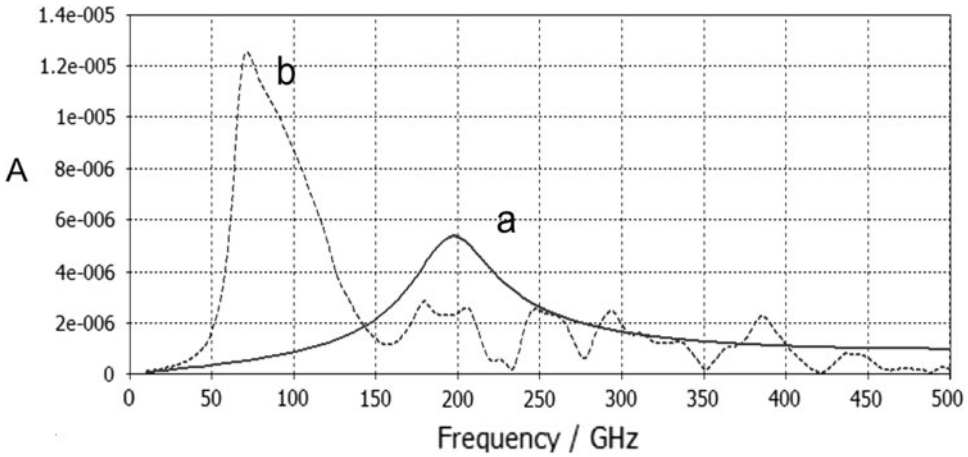

Fig. 5 The simulation of one linear thermocouple. **a** Free-standing, **b** lying on the structure shown in Fig. 4. The *vertical scale* shows the current in the middle contact

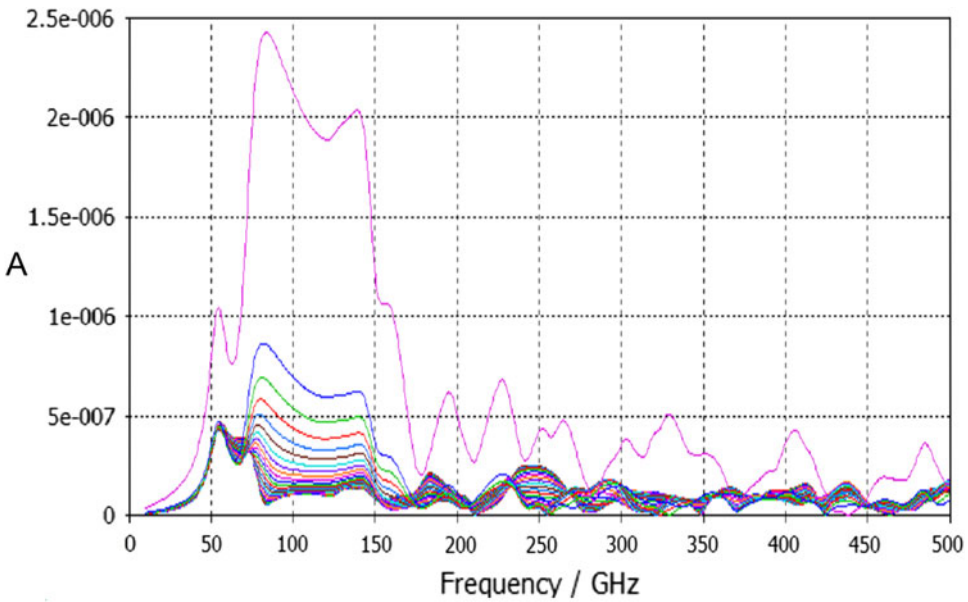

Fig. 6 The simulation of the complete structure. The current spectra in the in the thermocouple strips. The 1 spectrum regards to the strip at the edge and the 24 to the antenna in the middle of the structure

the incoming radiation at almost every frequency in an extremely wide bandwidth with a moderate first order resonance peak level while the thermocouples at the side parts have significant higher mode suppression with significant first order peak amplitude and bandwidth. Although it should be noted that even the highest resonant peak is only about ten times higher than the background. The currents in the strips are far lower than it is indicated in Fig. 5, however the combined efficiency of the 48 antennas are higher than that of one antenna. Simulation of the structure having a few less strips was performed and the result was very similar, the current in the outermost strip had a resonant peak, and these peaks decrease rapidly in the internal antennas. That is the peak is not due to the vicinity of the silicon substrate. The complete upper layer with the thermocouple strips behaves as conductor sheet.

The versions of the possible mounting were also investigated and compared to each other. Namely simulations were performed for the case when the chip is mounted on a dielectric plate (FR4 printed circuit board) instead of copper. These simulations resulted in higher currents in the central thermocouples, the average increment was 33%, and however in the strips at the edges this difference in mounting had no effect.

4 Measurements

The responsivity of the thermopile structure was characterized by direct electric heating of the loop-like structures using the integrated heater (see Fig. 3a) and the obtained value was 90 V/W. The thermal coefficient of the heater resistance was quantified from independent measurements and the temperature of the heated resistor was calculated by utilizing these results. Then the thermoelectric constant arising in the 40 p–n pairs was determined to be 18 mV/K. The response time of this structure was also measured by applying a square wave modulated heating current and observing the relaxation of the thermal voltage on the oscilloscope. A time of 9.3 ms was obtained.

For a first attempt the antenna-like operation was demonstrated in the K_u band at 13 GHz. The measurement proved that the device is capable of detecting microwave radiation with a responsivity of 5.6 V/W. The output signal depends strongly on the polarization of the radiation; the maximum was obtained when the microwave E-field was parallel to the strips, as shown in Fig. 7. In the THz band two measurements were performed: at 100 GHz and in a broad-band THz radiation. The 100 GHz signal was generated by successive multiplication of the microwave power and radiated to the chip by a W-band horn antenna. The broad-band THz signal was produced by the excitation of a non-linear crystal ($L_iN_bO_3$) by ps laser pulses. The

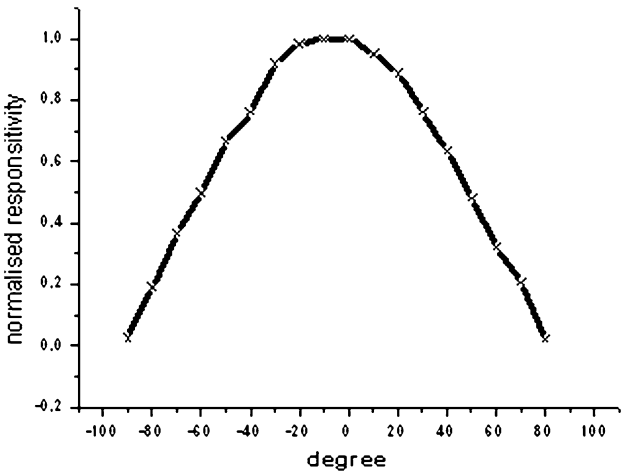

Fig. 7 The change of the output voltage when the chip rotated around the axe perpendicular to its surface. At 0° the E field of the 13 GHz radiation was parallel to the antenna strips

source provided ps impulses with an energy of 1.6 μJ energy, and a frequency of 1 kHz, adding up to a power of 1.6 mW for the broadband frequency region. The impulse itself and the spectra of the impulse are shown in Fig. 8. The radiation was focused to the sample by the appropriate optics. The spot size at the focus was about 2 mm. The intensity was regulated by the attenuator. The rotation of the chip in the THz radiation was not possible, however two positions were aligned: in the first the E field of the radiation was parallel to the strip antennas; in the second case it was perpendicular to them. In the later case no significant outputs over the noise were obtained. These strong polarisation dependencies support the functional principle; the connections do not result in any significant sensitivity in the orthogonal polarization.

Beyond these investigations the responsivity to infrared radiation was also measured. The source was a heated black body formed from a 5×5 cm^2 aluminium plate covered by "black velvet" paint (emissivity $\varepsilon \approx 1$). Its temperature was regulated by a controlled Peltier element between 0 and 100°C. The chip was placed 20 mm from the black surface, the radiation impinging on the detector was calculated from the Stefan–Boltzmann law considering the adequate view factor (Cengel and Ghajar 2010).

The responsivities were always calculated from the slope of the power- versus output voltage diagram to completely eliminate the zero offsets. The power was estimated from the chip area and the radiation intensity, i.e., the reflected and transmitted powers are unknown. The zero offset was rather high during the measurements at 100 GHz, because the operating temperature of the signal multiplayer was significantly over the room temperature and therefore the sensor responded to the infrared thermal radiation of the source as well. The measured responsivities

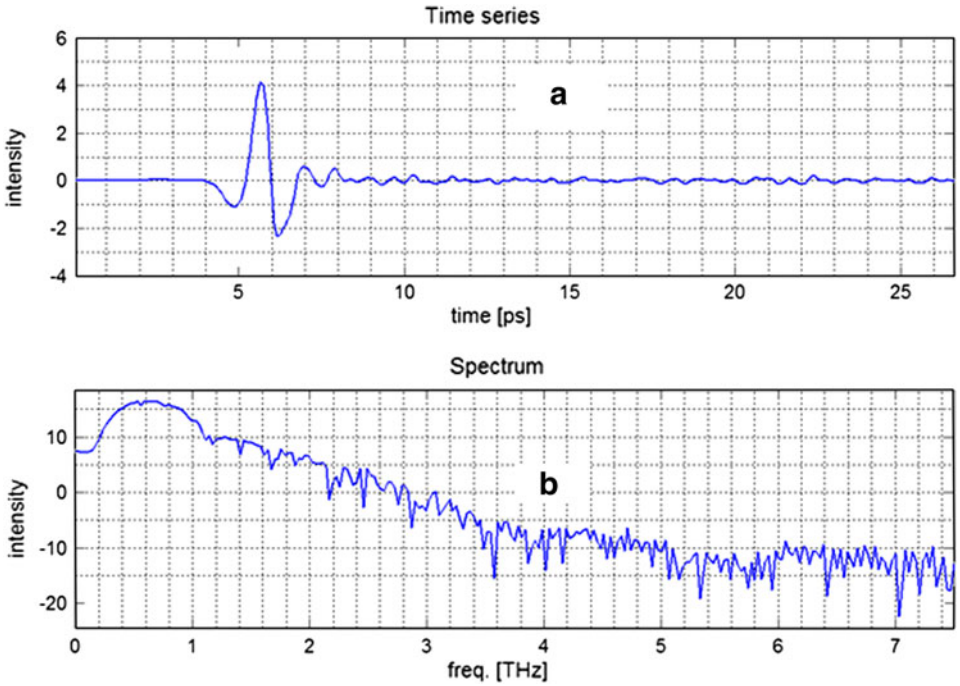

Fig. 8 **a** The broadband THz impulse. **b** The generated spectrum. The peak intensity lies around 600 GHz

on the same chip, shown in Fig. 3b, are listed in the Table 1

The kindred structure presented in Fig. 3a had the same responsivity to IR radiation and zero responsivity to the other excitations within the measurement uncertainty. The coupling factors are the ratios of the estimated responsivities and the 90 V/W, the responsivity to the direct electric heating, which can be considered as an absolute reference value. The recorded data clearly indicate that the efficiency increases with the increase of the frequency, further the responsivities to IR and to the broad-band THz are very close. The IR responsivity can be improved by applying some absorbing layers on the top of the device (Roncaglia et al. 2007); (Liddiard 1986). The coupling factor of the THz radiation is rather high, resulting in responsivity, comparable with other published values. (Chong and Ahmed 1997) obtained coupling factors in average 15%. The responsivities to electric heating was similar: 86 and 144 V/W for the different bolometers driven by 1 mA, from these data the THz responsivity could have been maximum 21 V/W. Kasalynas et al. (2007) described a thermopile detector matrix covered by absorbing film. Their maximum responsivity was obtained for TiN absorber; it was 28 V/W at 2.52 THz radiation. Minkevicius et al. (2011) published an InGaAs-based bow-type diode, it performed a responsivity of 6 V/W at 0.591 THz. (Öjefors et al. 2009) published a resonant on chip antenna and detector prepared by 0.25-μm CMOS technology for the 0.65 THz radiation. 150 V/W responsivity was reached at the resonant frequency, which is only about 0.2% of the simulated value.

The effect of mounting was also investigated experimentally in the broad-band THz radiation. Different equivalent chips (not that which is mentioned above) were mounted on copper plate and also on printed circuit board (FR4). The results are summarized in Table 2.

It seems that the average responsivities of the devices are about twice as high when they are mounted on the printed circuit board than the ones mounted onto the copper plate.

Table 1 The responsivities of the same chip to different excitations

Excitation	13 GHz	100 GHz	Broad-band THz	Thermal black-body radiation
Responsivity (V/W)	0.2	5.6	21	20
Coupling factor (%)	0.22	6.2	23.3	22.2

Table 2 The responsivities to the broad-band THz radiation of the different chips mounted on conducting and dielectric holder

Mark of the structure	4 × 2 A	Dip A 270	Dip A 375	Dip A 480
Length of the membrane (μm)	1,400	270	375	480
Average responsivity on Cu (V/W)	40.1	5.6	9.1	13.5
Average responsivity on FR4 (V/W)	76.5	14.9	23.5	30.2

Each structure contains 49 thermocouples

Table 3 The responsivities to the broad-band THz radiation of samples with different number of antennas, the dimensions and arrangements of the chips were identical, the size were 1 × 1 mm^2

Mark of the structure	DipB a	Dip B b	Dip B c
Number of strips	5	37	72
Strip width/spacing (μm)	20/60	10/10	5/5
Responsivity (V/W)	2	12.8	23
Average resistance (k Ω)	9.3	98.5	375
Thermal noise voltage (nV/$\sqrt{}$Hz)	12.2	39.7	77.5
Noise equivalent signal (nW/$\sqrt{}$Hz)	6.1	3.1	3.4

Each chip was mounted on an FR4 dielectric plate

This difference is somewhat higher than it was expected from the simulations, where the current was calculated to be about 33% higher in the case of using a dielectric plate instead of the copper in the model. Because the output thermal voltage is proportional to the absorbed power, i.e. the square of the current, an increment of about only 77% would be expected from the simulations. The chips marked by Dip A xxx differ only in the length of the membrane, all the other geometrical parameters are identical. Naturally the chip marked by 4 × 2 is longer. The measurements show the longer membranes perform higher responsivity.

Regarding the prospective encapsulation the cooling effect of the ambience was also estimated (Mancarella et al. 2006). Experiments applying internal direct heating and external thermal radiation were both repeated in vacuum. Significant improvement, by a factor of more than 3, of the responsivity was observed. Consequently heat transfer through air plays a substantial role during the measurements. Therefore the application of vacuum encapsulation would improve the performance of the device significantly.

Preliminary investigations were carried out on the layout of the sensor. Namely the effect of the number of antenna strips were also investigated, while the chip size remained unchanged, 1 × 1 mm^2. The inner hole under the membrane and the length of the p-n strips were also unvaried, 0.27 × 0.83 mm^2 and 0.62 mm, respectively. Table 3 summarizes the results of the characterizations using these three geometrically equivalent chips having different numbers of antenna.

We can conclude that the responsivity increases almost proportionally to the number of antennas, as it was indicated by the simulations as well; and even the noise limited sensitivity improves in spite of the increasing resistance. The detailed investigation of the optimum layout involving the sheet resistance is beyond the scope of this paper.

5 Conclusions

A novel construction of thermopile based THz sensor was investigated experimentally and theoretically by applying full wave electromagnetic simulations. The fundamental difference between this device and the traditional thermopile is the modified layout, namely the linear arrangement of the thermocouples. The basic operation of the device is analogue to a conventional bolometer, because the radiation power is absorbed in the structure. However, the working principle is based on the Seebeck effect hence no read-out current is required; in principle the output voltage is directly proportional to the detected signal and it is not only a small increment of the permanent voltage. A further advantage is that the heat generation peaks around the middle of the lines situated at the centre of the suspension membrane, exactly where it gives rise to the highest thermoelectric effect. The observed dependence of the output signal on the polarization of the radiation clearly proves the antenna-like functionality of the linear thermocouples. The comparative measurements implemented on the same chip demonstrate the improved responsivity at higher frequencies. The responsivity of the device exposed to electromagnetic radiation (THz and infrared) is only five times lower than when excited by direct electric heating. It should be noted, that this value was obtained without any absorbing coatings. The simulations described the current distribution in the active area of the sensor, and predicted a broadband sensitivity in the 100–500 GHz region. The responsivity and also the noise limited sensitivity increases with the number of the antenna strips. Regarding the future encapsulation: both the simulations and the measurements proved the advantage of the application of a dielectric mounting plate instead of a metallic one. The experiments in a vacuum ambient predict the significant improvement in the case of vacuum encapsulation.

Acknowledgments The measurements at 100 GHz were made at the Universität Duisburg-Essen, with the kind help of Vitaly Rymanov and Prof. Andreas Stöhr. The measurements with the broadband impulse THz source were performed at DESY, Hamburg with the valuable help and contribution of Matthias Hoffman. Their contribution is gratefully acknowledged. The authors thank the careful revision of the manuscript to Mr. Ádám Szendrényi and the kind support of Mr. László Nagy at the EnerSys Hungária Kft. The work was supported by CNK 77843 TERASTART OTKA grant.

References

Cengel YA, Ghajar AJ (2010) Heat and mass transfer: fundamentals and applications, 4th edn. McGraw-Hill, New York

Chong N, Ahmed H (1997) Antenna-coupled polycrystalline silicon air-bridge thermal detector for mid-infrared radiation. Appl Phys Lett 71:1607–1609

Dijkstra M, Lammerink TSJ, de Boer MJ, Berenschot JW, Wiegerink RJ, Elwenspoek MC (2008) Low-drift U-shaped thermopile flow sensor. In: IEEE sensors 2008 Conference, pp 66–69, 1-4244-2581-5/08/$20.00 ©2008 IEEE

Graf A, Arndt M, Sauer M, Gerlach G (2007) Review of micromachined thermopiles for infrared detection. Meas Sci Technol 18:R59–R75

Kasalynas I, Adamta AJL, Klaassena T, Hovenid NJ, Pandraudc G, Iordanovtc VP, Sarro PM (2007) Some properties of a room temperature THz detection array. Proc of SPIE 6596:65960J. doi:10.1117/12.726404

Liddiard KC (1986) Thin-film resistance bolometer IR detectors-II. Infrared Phys 26(1):43–49

Mancarella F, Roncaglia A, Cardinali GC (2006) A measurement technique for thermoelectric power of CMOA layers at the wafer level. Sens Actuators A 132:289–295

Minkevicius L, Tamosiunas V, Kasalynas I, Seliuta D, Valusis G, Lisauskas A, Boppel S, Roskos HG, Kőhler K (2011) Terahertz heterodyne imaging with InGaAs-based bow-tie diodes. Appl Phys Lett 99:131101

Öjefors E, Lisauskas A, Glaab DG, Roskos HG, Pfeiffer UR (2009) Terahertz imaging detectors in CMOS technology. J Infrared Milli Terahz Waves 30:1269–1280. doi:10.1007/s10762-009-9569-4

Resnik D, Aljančič U, Vrtačnik D, Možek M, Amon S (2004) Mechanical stress in thin film microstructures on silicon substrate. Vacuum 73:623–628

Roncaglia A, Mancarella F, Cardinali GC (2007) CMOS-compatible fabrication of thermopiles with high sensitivity in the 3–5 μm atmospheric window. Sens Actuators B 125:214–223

Seidel H, Csepregi L, Heuberger A, Baumgärtel H (1990) Anisotropic etching of crystalline silicon in alkaline solutions. J Elchem Soc 137:3612–3625

Szabó PG, Székely V (2009) Characterization and modeling of electro-thermal MEMS structures. Microsyst Technol 15: 1293–1301

Szentpáli B, Basa P, Fürjes P, Battistig G, Bársony I, Károlyi G, Berceli T, Rymanov V, Stöhr A (2010) Thermopile antennas for detection of millimeter waves. Appl Phys Lett 96:133507

Vázsonyi É, Vértesy Z, Tóth A, Szlufcik J (2003) Anisotropic etching of silicon in a two-component alkaline solution. J Micromech Microeng 13:165–169